Geophysical Journal International

Geophys. J. Int. (2021) **225,** 548–554
Advance Access publication 2020 December 21
GJI Seismology

doi: 10.1093/gji/ggaa603

The development of seismic anisotropy below south-central Alaska: evidence from local earthquake shear wave splitting

E. Karlowska [1,2] I. D. Bastow,[1] S. Rondenay,[3] R. Martin-Short[2] and R. M. Allen[2]

[1] *Department of Earth Science and Engineering, Imperial College London, London SW 7 2BP, UK. E-mail: i.bastow@imperial.ac.uk*
[2] *Seismological Laboratory, University of California, Berkeley, CA 94720, USA*
[3] *Department of Earth Science, University of Bergen, N-5020 Bergen, Norway*

Accepted 2020 December 11. Received 2020 December 8; in original form 2020 September 11

SUMMARY

The Transportable Array in south-central Alaska spans several subduction zone features: backarc, forearc and volcanic arc, making it an ideal tool to study subduction zone anisotropy. Shear wave splitting analysis of 157 local earthquakes of $m_b \geq 3.0$ that occurred between 2014 and 2019 yields 210 high-quality measurements at 23 stations. Splitting delay times (δt) are generally small ($\delta t \approx 0.3$ s), increasing with distance from the trench. Arc-parallel fast directions, ϕ, are only seen in the forearc, but rotate to arc-perpendicular ϕ in the backarc. Observed ϕ values generally do not parallel teleseismic SKS splitting results, implying that the latter is sensitive primarily to subslab mantle flow, not mantle wedge dynamics. The forearc local-earthquake signal likely originates from anisotropic serpentinite in fractures atop the subducting Pacific Plate, with possible additional signal coming from fractures in the North American crust. Mantle wedge corner flow, potentially with additional arc-perpendicular anisotropy in the subducting slab, explains backarc anisotropy.

Key words: North America; Seismic anisotropy; Subduction zone processes; Volcanic arc processes.

1 INTRODUCTION

The processes operating along the >50 000 km length of Earth's subduction zone system are debated. In the mantle, 3-D along-arc flow, 2-D corner flow and complex toroidal flow patterns at slab edges have variously been hypothesized in different settings (e.g. Long & Silver 2008; Abt *et al.* 2009). Fracture systems in the downgoing and overriding plate, with or without a thin serpentinite layer atop the downgoing plate (Abers *et al.* 2017), may also characterize some subduction zones (see Long 2013, for a review). Key to resolving these tectonic and geodynamic subduction zone characteristics is the measurement of seismic anisotropy, the directional dependence of seismic wave speed. Much subduction zone anisotropy is expected to result from the development of lattice preferred orientation (LPO) fabrics in crust and mantle minerals such as olivine. However, b-type, as opposed to the more common a-type, c-type or e-type, olivine LPO (Karato *et al.* 2008) can develop when mantle wedge conditions are suitably high differential stress and low temperature (e.g. Zhang & Karato 1995). This changes the relationship between strain, crystal alignment and the resulting anisotropy: the flow is perpendicular to the anisotropic fast direction, not parallel to it (e.g. Nakajima & Hasegawa 2004; Kneller *et al.* 2005).

Shear wave splitting utilizes the observation that when a shear wave encounters an anisotropic medium, it splits into two orthogonal shear waves: from local earthquakes one travelling faster than the other (e.g. Silver & Chan 1991). The splitting is quantified by the time delay (δt) between the two shear waves and the orientation (ϕ) of the fast shear wave. Key to resolving different sources of seismic anisotropy at subduction zones is analysis of shear wave splitting in a variety of waveforms, including both teleseismic (e.g. SKS) and *S* wave from local earthquakes: the former are path averages of the entire upper mantle below a station; the latter afford resolution of shallower anisotropic fabrics.

Local *S*-wave splitting studies often reveal an arc-parallel to arc-perpendicular transition in ϕ from the forearc to the backarc (e.g. Tonga: Smith *et al.* 2001; Middle America: Abt *et al.* 2009). Some studies, however, report only arc-parallel directions [e.g. Long & Silver 2008 (various locations); the Caribbean: Piñero-Feliciangeli & Kendall 2008; the Aleutians: Yang *et al.* 1995] or only arc-perpendicular directions (e.g. Scotia: Müller 2001); elsewhere, more complex patterns are observed (e.g. Kamchatka: Levin *et al.* 2004). Measurements of δt from local *S* waves also vary between subduction zones worldwide: $\delta t \approx 0.3 \pm 0.4$ s at the Hikurangi subduction zone (Morley *et al.* 2006); $\delta t \approx 0.8 \pm 0.5$ s at Ryukyu (Long & van der Hilst 2006); and $\delta t \approx 1.5 \pm 0.4$ s at the Aleutians (Long & Silver 2008). Smaller delay times are sometimes cited as evidence that a strong mantle wedge flow field is lacking, and vice versa (e.g. Long 2013).

South-central Alaska, where 50 mm yr^{-1} (Sauber *et al.* 1998) northward-verging subduction of the Pacific Plate is ongoing beneath North America, is an ideal study locale for subduction zone dynamics because recent deployment of the Transportable Array (TA) network spans both forearc and backarc settings (Fig. 1). Previous SKS splitting studies in this part of Alaska have suggested toroidal mantle flow as the dominant cause of the observations (Christensen & Abers 2010; Hanna & Long 2012; Venereau *et al.* 2019). Most recently, the SKS splitting study of McPherson *et al.* (2020) corroborates this view, except below the Kenai Peninsula, where they suggest that there is likely little-to-no mantle above the plate interface. However, source-side splitting analysis (Walpole *et al.* 2017) suggests that the SKS signal originates from below, not above, the subducting slab. To address this debate, and to better constrain sources of anisotropy beneath the region, we perform a shear wave splitting study of local earthquakes in Alaska.

2 LOCAL EARTHQUAKE DATA SET AND SHEAR WAVE SPLITTING METHODOLOGY

Seismograms of magnitude $m_b \geq 3.0$ and depth 10–212 km earthquakes in the region 55–66.5°N, 142–166°W occurring between January 2014 and April 2019 were obtained from the IRIS Data Management Center for 23 TA broad-band stations. From this initial data set, a total of 814 earthquake–station pairs were examined for which the *S*-wave incident angle is within the shear wave window (SWW). The SWW is the vertical cone bound by $i_c = \sin^{-1}(V_s/V_p)$, where *S*-wave particle motions are not disturbed by *P* head wave and *S*–*P* conversions at the free surface (Booth & Crampin 1985). A zero-phase Butterworth bandpass filter with corner frequencies of 0.1–1.0 Hz was applied to all seismograms. This frequency range is similar to that adopted in analogous local earthquake shear wave splitting studies (e.g. Long & van der Hilst 2006).

Splitting analysis was carried out using the method of Teanby *et al.* (2004), which is based on the traditional Silver & Chan (1991) method, with errors estimated using the method of Walsh *et al.* (2013). Horizontal components are rotated and time-shifted to minimize the second eigenvalue of the covariance matrix for particle motion within a time window around the shear wave arrival. This process is similar to linearizing the particle motion and minimizing tangential component shear wave energy. The traditional Silver & Chan (1991) approach takes a single, manually picked, shear wave analysis window. In the cluster analysis approach of Teanby *et al.* (2004), the splitting analysis is performed for a range of window lengths and cluster analysis is utilized to find measurements that are stable over many different windows. All splitting parameters were determined after analysis of 100 different windows: each window encapsulates at least a full cycle of *S*-wave energy, with the range of window start and end times spanning approximately half to a full wavelength—sufficient to resolve splitting that results in elliptical or cruciform particle motion (the latter can result when δt is comparable to the wavelength of the *S*-wave energy; e.g. Booth & Crampin 1985). The result chosen by the cluster algorithm is the one from the most stable cluster with the lowest error (calculated via an *F*-test to obtain the 95 per cent confidence interval). An example high-quality splitting result is shown in Supporting Information Fig. S1.

Some studies (e.g. Saltzer *et al.* 2000; Wirth & Long 2010) have demonstrated a bias towards near-surface layers in high-frequency splitting results. The filter bands used in our local splitting analysis overlap with the SKS studies [e.g. Venereau *et al.* (2019) used 0.04–0.3 Hz compared to our 0.1–1 Hz), so we expect frequency-dependent effects to be minimal in our study. Nevertheless, we attempted splitting analysis of both local and SKS waveforms for stations M22K, O19K and O20K using filter corner frequencies of 0.1–0.5 Hz. This reduced the high-frequency content of the local earthquake data set, and pushed the SKS analysis to higher frequencies. For almost all local earthquakes, evidence for coherent shear wave energy from which acceptable quality splitting measurements could be made was lacking. Three exceptions to this rule yielded local earthquake splitting results that showed no clear change in ϕ, but a slight increase in δt and associated errors (e.g. from 0.38 ± 0.03 to 0.55 ± 0.05 s at O20K), notably still much lower delay times than in the published SKS data sets from the region. For the SKS data set, splitting analysis in the frequency range 0.1–0.5 Hz was attempted for the same station–earthquake pairs as Venereau *et al.* (2019) for stations M22K, O19K and O20K (Supporting Information Table S2). For four of the original seven earthquakes where an acceptable quality measurement could be obtained, we found near-identical splitting parameters as for the 0.04–0.3 Hz range.

3 RESULTS

We obtained 210 splitting measurements at 23 TA stations from 157 earthquakes of depth 18–204 km. Arc-parallel ϕ results are generally only observed in the forearc; arc-perpendicular ϕ directions dominate the backarc (Fig. 1). Observations of δt range from 0.10 to 0.96 s; 96 per cent are $\leq$0.5 s, with an average 0.32 ± 0.03 s (Supporting Information Table S1). Our results have errors $\sigma_\phi \leq 13.75°$ and $\sigma_{\delta t} \leq 0.17$ s. As expected, δt generally increases with path length [calculated by ray tracing through the ak135 velocity model of Kennett *et al.* (1995); Fig. 2], so we calculate per cent anisotropy by dividing δt with ak135 predicted *S*-wave traveltimes. Anisotropy is almost exclusively <3 per cent across the network, with an average of 1.04 per cent. Stations O19K and O20K account for ~2/5 of all measurements. Increased seismicity there is attributable to the curvature of a subducting slab (e.g. Ratchkovski & Hansen 2002). Most of the earthquakes within the SWW were located in south-central Alaska. A few events in the SWW north of 53°N were, unfortunately, of too low signal-to-noise ratio to conduct a reliable shear wave splitting analysis. Maps showing per cent anisotropy, rather than δt (Fig. 1), are shown in Supporting Information Fig. S2.

Fabric type can have a big impact on splitting parameters for non-vertical *S*-wave phases (e.g. Savage 1999). Approximately 1/3 of our *S* waves have incidence angles (θ) <20°; 95 per cent are <35°. Examining splitting delay times as a function of θ, we find that $\delta t_{\theta<20°} = 0.306$ s, ranging from 0.12 to 0.53 s; $\delta t_{\theta>20°} = 0.322$ s, ranging from 0.1 to 0.96 s. Performing a Kolmogorov–Smirnov test on the two i_c families of data reveals that they are near-identical, with a high *P*-value of 58 per cent indicating that we cannot preclude the hypothesis that the two data sets sample the same distribution.

4 DISCUSSION

4.1 Causes of seismic anisotropy and comparison to previous studies

A striking observation in Fig. 1 is the lack of correlation between our local earthquake-derived ϕ directions and SKS splitting results. Corroborating earlier studies (Christensen & Abers 2010; Hanna

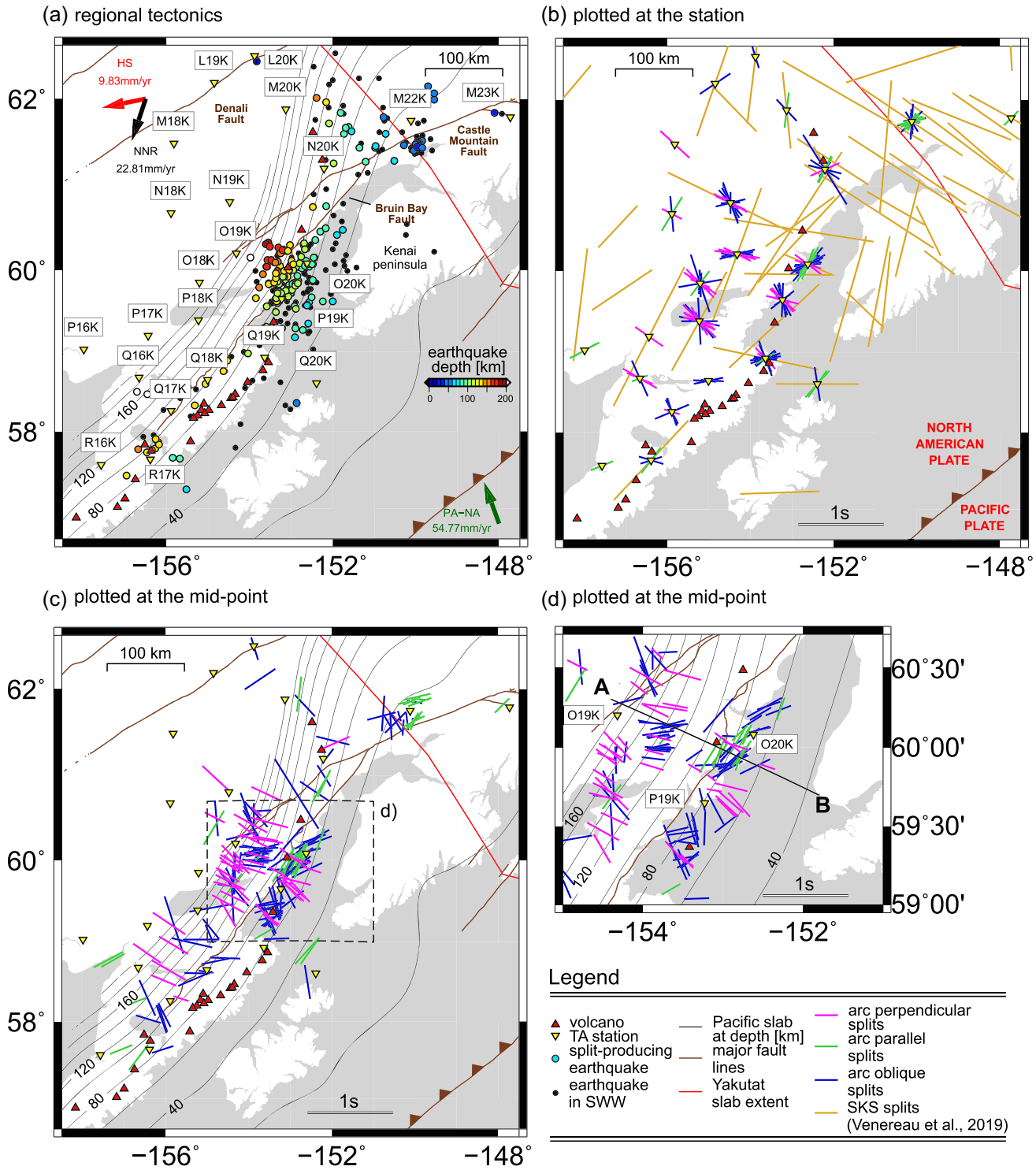

Figure 1. (a) Tectonic setting of south-central Alaska with major fault lines (Colpron *et al.* 2007), TA seismograph stations and earthquakes (circles) that produced high-quality splitting measurements. Solid arrows: absolute plate motion (APM) in the hot spot (HS) and no-net-rotation (NNR) reference frames (Gripp & Gordon 2002). Slab2.0 contours are after Hayes *et al.* (2018). (b) Local *S*-wave splitting measurements in south-central Alaska plotted at the station. (c) As per (b), but plotted at the ray-path midpoint. (d) Close-up of stations O19K and O20K plotted at the ray-path midpoint.

& Long 2012), Venereau *et al.* (2019) suggested that mantle flow above the subducting Pacific Plate was a primary cause of SKS anisotropy in the region; the later SKS study of McPherson *et al.* (2020) generally supports this view, but adopted a subslab mantle flow hypothesis to explain observations in the Kenai Peninsula area where they point out that there is likely little-to-no mantle above the plate interface. The anticorrelation of our ϕ observations with the SKS studies may indicate that the SKS data set is sensitive primarily to intraslab or subslab anisotropy. Corroborating this hypothesis, the recent source-side splitting global study of Walpole *et al.* (2017),

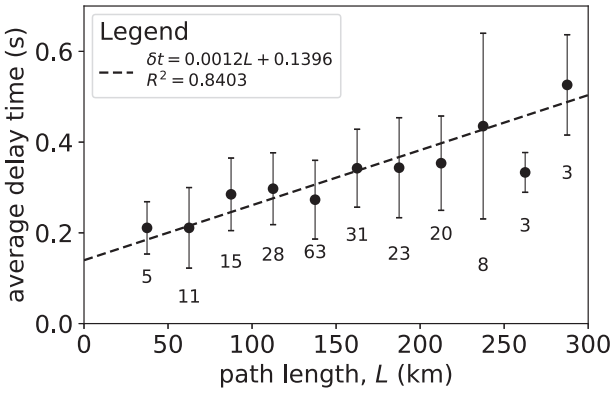

Figure 2. Average splitting delay times (δt) for 25 km bins of path length, L. Path length is calculated assuming ray paths through the ak135 mode of Kennett *et al.* (1995). Error bars show the standard deviation of the delay times in each bin, with the contribution of each weighted by its signal-to-noise ratio. Numbers below each data point are the number of measurements contributing to each bin. The dashed line is a linear, least-squares fit, showing an increasing trend in average delay time with path length.

which is inherently biased towards subslab anisotropy in subduction zones, presents ϕ and δt observations for Alaska akin to the SKS studies, at least in the area where our local and SKS splitting comparisons are being made. On the other hand, a similar study of source-side splitting by Lynner & Long (2014) found somewhat scattered ϕ observations below Alaska, albeit with a weak trend in ϕ that aligns approximately with the subducting plate motion. They attributed much of the scatter to the significant distances ray paths travel through the slab below Alaska, in contrast to other regions of source-side study such as Central America where signal contamination from the slab is not so apparent.

Comparing values of δt for local earthquakes and SKS arrivals has to be done cautiously because there can be a demonstrable bias towards near-surface structure in local earthquake analyses. Specifically, δt has, in some areas, been shown to decrease at higher frequencies (e.g. Marson-Pidgeon & Savage 1997; Wirth & Long 2010), with near-surface anisotropic regimes contributing more at higher frequencies (e.g. Saltzer *et al.* 2000). With this caveat in mind, it is nevertheless interesting to note that we constrain markedly smaller δt values than the SKS studies [$\delta t \approx 0.32$ s here; e.g. Venereau *et al.* (2019) found $\delta t_{SKS} \approx 1.19$ s). Our local earthquake δt observations can therefore be used cautiously to corroborate the hypothesis that the SKS and local earthquake data sets are dominated by different anisotropic layers.

High aspect ratio melt inclusions generally result in higher per cent anisotropy than we observe, so we do not favour that hypothesis for Alaska (e.g. Keir *et al.* 2005; Bastow *et al.* 2010). Our δt observations also contrast with larger ones at some other subduction zones, where hypotheses of mantle wedge flow have been favoured. For example, Smith *et al.* (2001) interpreted $\delta t \approx 1.3 \pm 0.3$ s in Tonga as along-arc mantle flow; Long & van der Hilst (2006) cited $\delta t \approx 0.8 \pm 0.5$ s as evidence for a 2-D wedge corner flow below Ryukyu. Large δt times are not globally ubiquitous; however, δt observations akin to ours have been noted in the Caribbean (Piñero-Feliciangeli & Kendall 2008) and South America (Polet *et al.* 2000), with these studies generally arguing against mantle wedge flow. Yang *et al.* (1995) suggest that the crust contributes $\delta t \approx 0.1$ s to the 0.1–0.35 s total δt observed beneath the Aleutians. However, Alaskan forearc and backarc structural trends do not mirror the abrupt change in ϕ (Fig. 1), so a continental crustal origin for the anisotropy is not an obvious candidate to explain the results. Few stations in our study are perfectly suited to an isolated study of anisotropy in the 50 km thick (e.g. Martin-Short *et al.* 2018) upper plate. However, M22K within the Yakutat terrane, where there is little-to-no mantle wedge, is well placed for such analysis: δt ranges from 0.11s for the shallowest earthquakes to 0.32 s for those exceeding 100 km depth; ϕ parallels surface geological trends. With a mean of $\delta t = 0.21$ s at M22K, it is clear that the North American upper plate contributes some signal to our observations, but also that it generally does not dominate them, particularly where ϕ shows no parallelism with geological trends. Intriguingly, δt shows a gentle increase of ∼0.33 s with path length over ∼300 km (Fig. 2). In central America, Abt *et al.* (2009) constrained similar δt patterns to those observed here (∼0.3 s over ∼200 km), and attributed it to mantle wedge anisotropy.

4.2 Forearc anisotropy

We see some evidence for arc-perpendicular and subperpendicular anisotropy in the Alaskan forearc (Fig. 1); perhaps the result of fabrics in the subducting slab itself. Tian & Zhao (2012), for example, found evidence for arc-perpendicular anisotropy in the subducting Pacific Plate, which they interpreted to originate from mid-ocean ridge formation. However, there is also evidence for arc-parallel anisotropy in the Alaskan forearc (Figs 1b and c), with station O20K particularly well located for analysis of this signature (Fig. 1d). In some cases, ϕ parallels geological trends, so we cannot preclude the possibility that some splitting (∼ 0.2 s) is accrued in the North American crust (Fig. 2). Indeed, in their anisotropic *P*-wave tomography study, Gou *et al.* (2019) found some evidence for arc-parallel ϕ in our study area. However, the aforementioned abrupt transition to arc-perpendicular anisotropy northwest of O20K, despite the lack of change in structural trends, argues for a deeper contribution to the observations.

Abers *et al.* (2017) suggests that the O20K region lies above a cold mantle wedge 'nose' that is decoupled from the core of mantle wedge (Fig. 3). The arc-parallel anisotropy we observe is therefore unlikely the result of flow in the mantle wedge. When reviewed in light of the *P*- and *S*-wave study of Tian & Zhao (2012), which found no evidence for anisotropy in Alaska's cold mantle wedge nose, we conclude that our O20K results are unlikely to be influenced by mantle flow, which likely only dominates further away from the arc (Gou *et al.* 2019).

Arc-parallel anisotropy can result from arc-parallel faults in a serpentinite layer on the top of subducting slabs (Faccenda *et al.* 2008): for short (10 km long) faults, such a layer can produce $\delta t \approx$ 0.26–0.35 s, similar to the mean $\delta t \approx 0.32 \pm 0.03$ s we observe. A serpentinite layer is expected to form if the forearc mantle is sufficiently hydrated by water released by the downgoing slab. Corroborating the Abers *et al.* (2017) view that the Alaskan mantle wedge is only moderately hydrated, using receiver function constraints on V_p/V_s ratios, Rossi *et al.* (2006) estimated the extent of serpentinization in the Alaskan mantle wedge to be <30 per cent for slab depths <80 km. Further constraints on mantle wedge serpentinization come from recent tomographic imaging studies in the region (e.g. Martin-Short *et al.* 2016, 2018; Berg *et al.* 2020) that image low wave speeds atop the subducting Pacific Plate slab. Berg *et al.* (2020), however, suggest low serpentinization and moderate mantle wedge hydration below Alaska. The low wave speeds may therefore instead be the result of other subduction zone processes, such as inclusion of crustal velocity material in the wedge. The

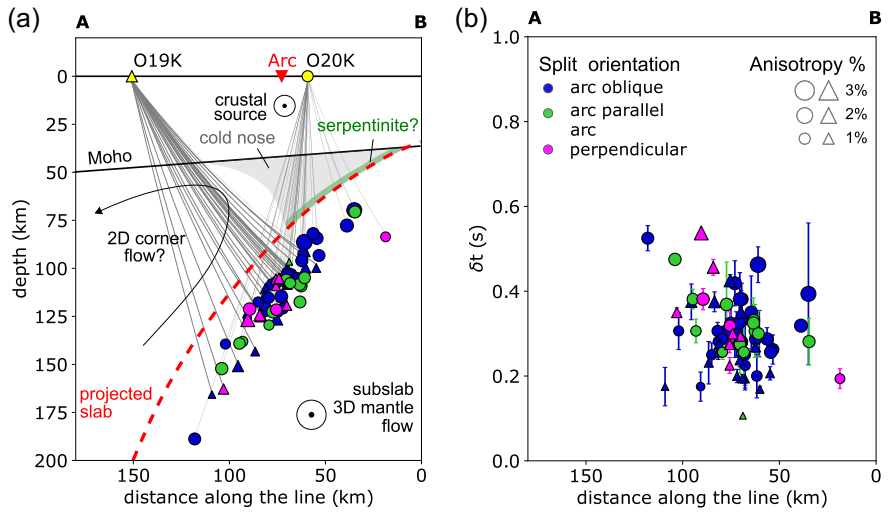

Figure 3. (a) Earthquakes producing splits at stations O19K (triangles) and O20K (circles), projected onto line A–B in Fig. 1(d). Subducting upper slab extent is after Hayes *et al.* (2018). Moho depths are after Martin-Short *et al.* (2018). The cold nose extent is after Abers *et al.* (2017). The projected ray paths are calculated according to the ak135 velocity model of Kennett *et al.* (1995). (b) Splitting delay times projected onto line A–B, showing a ∼0.3 s increase in δt away from the trench.

serpentine in faults hypothesis for the O20K splitting observations is thus not unambiguous. Additionally, we cannot completely rule out the possibility of b-type olivine fabrics here (e.g. Kneller *et al.* 2005). However, the *P*-wave study of Gou *et al.* (2019) presented ample evidence for anisotropy in the crust and subducting slab below this region, but little-to-none in the mantle wedge. Therefore, we propose that anisotropy in the forearc region is likely produced by a combination of anisotropy in the downgoing plate, a thin layer of serpentinite on top of the slab and/or the North American crust, with minimal influence from the mantle wedge itself.

4.3 Backarc anisotropy and implications for subslab mantle flow

Station O19K is well placed to examine backarc anisotropy below Alaska (Figs 1 and 3). In general, ϕ is perpendicular to geological trends, so we rule out continental crustal anisotropy as the dominant explanation for our results. Alaska's cold mantle wedge nose ends <100 km from where the North American crust meets the nose tip (Abers *et al.* 2017; Fig. 3a). Backarc results at O19K, and elsewhere, are therefore too distant from the trench to be sampling b-type olivine fabrics, which are only thought to develop in the cold 'nose' of the mantle wedge (e.g. Song & Kawakatsu 2013). Assuming a-type (or c-type or e-type) olivine LPO, our arc-perpendicular observations may therefore be illuminating a 2-D corner flow, as previously proposed by Long & Silver (2008). Supporting this hypothesis, δt increases away from the trench (Fig. 3b). It is notable that our δt observations are smaller than those in the backarc regions of some other subduction zones. For example, Long & van der Hilst (2006) found $\delta t \approx 0.8$ s in their study of Ryukyu. With the caveat that frequency-dependent effects may be exerting strong control on δt in our study, our smaller delay times are perhaps the result of a thinner corner flow anisotropic layer: Alaska has a thicker upper plate [∼50 km (Martin-Short *et al.* 2018) compared to 35–40 km in Ryukyu (Taira 2001)] and generally shallower earthquakes [∼114 km compared to ∼145 km in Long & van der Hilst (2006)] in the less steep Alaskan slab. However, we acknowledge the obliquity of subduction in the Cook Inlet area, so the 2-D corner flow assumption may be overly simplistic here. Indeed, Kneller & Van Keken (2007, 2008) model complex flow patterns above oblique, curved and varying-dip slabs and highlight the potential for complex resulting anisotropic patterns: along-strike variations in slab geometry lead to trench-parallel pressure gradients and are thus a possible mechanism for 3-D flow (e.g. Kneller & Van Keken 2008). Several of our splitting observations show evidence for arc obliquity (Figs 1 and 3), implying some departure from simple 2-D flow models is likely. Future studies of Alaskan anisotropy could usefully tackle the challenge of carrying out 3-D modelling to further pinpoint the likely variations in wedge and subslab flow patterns. Specifically, the influence of Alaska's variable slab dip, slab curvature, oblique subduction and slab edge would all need to be considered carefully.

As indicated earlier, our local earthquake splitting observations suggest a substantial subslab contribution to the SKS data sets of Venereau *et al.* (2019) and McPherson *et al.* (2020). McPherson *et al.* (2020) already support this hypothesis for the Kenai Peninsula, where there is likely little-to-no mantle above the plate interface. Our observations are also not easily explained by the mantle flow hypothesis of Jadamec & Billen (2010) who, consistent with SKS measurements more broadly in Alaska, predict strong mantle wedge flow due to the proximity of the slab edge in Alaska and its influence in generating a toroidal mantle flow field.

Studies of subslab anisotropy do exist. For example, Faccenda & Capitanio (2013) modelled the development of LPO in olivine–enstatite aggregates in a 3-D slab rollback flow field. They proposed two zones of subslab anisotropy. At shallow depths, simple shear beneath the slab generates a ≥100 km thick layer of arc-normal ϕ. At greater depths, the fast axes remain arc normal but plunge parallel to the subducting slab. This layer systematically overlies a deeper layer, or 'core' of arc-parallel ϕ, generated by pure shear in the slab retreat direction. This anisotropic core is strongest near slab edges, as per our study area, where the divergence of the horizontal subslab flow is greatest. Such a geodynamic scenario, which has been suggested as appropriate for the Aegean, for example (Olive *et al.* 2014), seems inappropriate for Alaska given the largely arc-parallel fast directions in the SKS data set SW of the slab edge (Fig. 1b). Instead, subduction of the oceanic asthenosphere may be the dominant source of subslab anisotropy in our study area, as has

been suggested by Song & Kawakatsu (2013) for central Alaska. Either way, further modelling of the SKS data set would be needed to confirm or refute any subslab hypothesis, which our data set is inherently incapable of resolving.

A combination of shallower 2-D corner flow and deeper 3-D toroidal flow has been suggested in Cocos subduction zone (Soto *et al.* 2009). To this end, the observed discrepancy between the SKS and local *S*-wave data sets in south-central Alaska could simply be due to the data sets being sensitive to different parts of mantle wedge. Our local *S*-wave splitting results may be sensitive to a relatively small-scale shallow 2-D corner flow, while the SKS data sets are sensitive to deeper 3-D flow (Jadamec & Billen 2010; Venereau *et al.* 2019); additional arc-perpendicular anisotropy in the subducting slab may contribute to both. However, the Cook inlet segment is quite some distance from the slab edge, and geodynamic modelling suggests that toroidal flow may not dominate this far south (e.g. Jadamec & Billen 2010).

5 CONCLUSIONS

We report weak shear wave splitting from earthquakes in south-central Alaska with $\delta t = 0.10$–0.96 s, with δt generally increasing away from the trench. In ϕ, we observe an arc-parallel to arc-perpendicular forearc to backarc transition. With some local exceptions (e.g. M22K and O20K), continental crustal structural trends cannot generally explain the observations, suggesting a deeper anisotropic source. Forearc anisotropy region is likely produced by a combination of the downgoing plate, a thin layer of serpentinite on top of the slab and/or North American crust, with relatively little influence from the mantle wedge. Backarc results indicate a 2-D corner flow in the presence of a-type olivine LPO (potentially with additional arc-perpendicular anisotropy in the subducting slab), akin to the Long & Silver (2008) hypothesis for mantle wedge flow in Alaska. If correct, our interpretations imply that SKS splitting results for the Kenai Peninsula region of south-central Alaska are explained best by subslab mantle flow, not flow in the mantle wedge.

ACKNOWLEDGEMENTS

Two anonymous reviewers provided helpful feedback that prompted us to think more deeply about our results. Seismograms come from the Incorporated Research Institutions for Seismology Data Management Center, which is funded through the Seismological Facilities for the Advancement of Geoscience and EarthScope (SAGE) Proposal of the National Science Foundation under Cooperative Agreement EAR-126168. TA network data were made freely available as part of the EarthScope USArray facility, operated by IRIS and supported by the National Science Foundation, under Cooperative Agreements EAR-1261681 (Busby & Aderhold 2020). IB acknowledges support from Natural Environment Research Council Grant NE/S014136/1.

REFERENCES

Abers, G., Van Keken, P. & Hacker, B., 2017. The cold and relatively dry nature of mantle forearcs in subduction zones, *Nat. Geosci.,* **10**(5), 333–337.

Abt, D.L., Fischer, K.M., Abers, G.A., Strauch, W., Protti, J.M. & González, V., 2009. Shear wave anisotropy beneath Nicaragua and Costa Rica: implications for flow in the mantle wedge, *Geochem. Geophys. Geosyst.,* **10**(5), doi:10.1029/2009GC002375.

Bastow, I., Pilidou, S., Kendall, J.-M. & Stuart, G., 2010. Melt-induced seismic anisotropy and magma assisted rifting in Ethiopia: evidence from surface waves, *Geochem. Geophys. Geosyst.,* **11,** doi:10.1029/2010GC003036.

Berg, E.M., Lin, F.-C., Allam, A., Schulte-Pelkum, V., Ward, K.M. & Shen, W., 2020. Shear velocity model of Alaska via joint inversion of Rayleigh wave ellipticity, phase velocities, and receiver functions across the Alaska Transportable Array, *J. geophys. Res.,* **125**(2), doi:10.1029/2019JB018582.

Booth, D. & Crampin, S., 1985. Shear-wave polarizations on a curved wavefront at an isotropic free surface, *Geophys. J. Int.,* **83**(1), 31–45.

Busby, R.W. & Aderhold, K., 2020. The Alaska Transportable Array: as built, *Seismol. Res. Lett.,* **91,** 3017–3027.

Christensen, D. & Abers, G., 2010. Seismic anisotropy under central Alaska from SKS splitting observations, *J. geophys. Res.,* **115**(B4), doi:10.1029/2009JB006712.

Colpron, M., Nelson, J. & Murphy, D., 2007. Northern Cordilleran terranes and their interactions through time, *GSA Today,* **17**(4/5), 4–10.

Faccenda, M. & Capitanio, F., 2013. Seismic anisotropy around subduction zones: insights from three-dimensional modeling of upper mantle deformation and SKS splitting calculations, *Geochem. Geophys. Geosyst.,* **14**(1), 243–262.

Faccenda, M., Burlini, L., Gerya, T.V. & Mainprice, D., 2008. Fault-induced seismic anisotropy by hydration in subducting oceanic plates, *Nature,* **455**(7216), 1097–1100.

Gou, T., Zhao, D., Huang, Z. & Wang, L., 2019. Aseismic deep slab and mantle flow beneath Alaska: insight from anisotropic tomography, *J. geophys. Res.,* **124**(2), 1700–1724.

Gripp, A.E. & Gordon, R.G., 2002. Young tracks of hotspots and current plate velocities, *Geophys. J. Int.,* **150**(2), 321–361.

Hanna, J. & Long, M.D., 2012. SKS splitting beneath Alaska: regional variability and implications for subduction processes at a slab edge, *Tectonophysics,* **530,** 272–285, doi:10.1016/j.tecto.2012.01.003.

Hayes, G.P., Moore, G.L., Portner, D.E., Hearne, M., Flamme, H., Furtney, M. & Smoczyk, G.M., 2018. Slab2, a comprehensive subduction zone geometry model, *Science,* **362**(6410), 58–61.

Jadamec, M.A. & Billen, M.I., 2010. Reconciling surface plate motions with rapid three-dimensional mantle flow around a slab edge, *Nature,* **465**(7296), 338–341.

Karato, S.-I., Jung, H., Katayama, I. & Skemer, P., 2008. Geodynamic significance of seismic anisotropy of the upper mantle: new insights from laboratory studies, *Annu. Rev. Earth Planet. Sci.,* **36**(1), 59–95.

Keir, D., Kendall, J.-M., Ebinger, C. & Stuart, G., 2005. Variations in late syn-rift melt alignment inferred from shear-wave splitting in crustal earthquakes beneath the Ethiopian rift, *Geophys. Res. Lett.,* **32**(23), doi:10.1029/2005GL024150.

Kennett, B.L.N., Engdahl, E.R. & Buland, R., 1995. Constraints on seismic velocities in the Earth from traveltimes, *Geophys. J. Int.,* **122**(1), 108–124.

Kneller, E. & Van Keken, P., 2007. Trench-parallel flow and seismic anisotropy in the Mariana and Andean subduction systems, *Nature,* **450**(7173), 1222–1225.

Kneller, E. & Van Keken, P., 2008. Effect of three-dimensional slab geometry on deformation in the mantle wedge: implications for shear wave anisotropy, *Geochem. Geophys. Geosyst.,* **9**(1), doi:10.1029/2007GC001677.

Kneller, E., Van Keken, P.E., Karato, S.-I. & Park, J., 2005. B-type olivine fabric in the mantle wedge: insights from high-resolution non-Newtonian subduction zone models, *Earth planet. Sci. Lett.,* **237**(3–4), 781–797.

Levin, V., Droznin, D., Park, J. & Gordeev, E., 2004. Detailed mapping of seismic anisotropy with local shear waves in southeastern Kamchatka, *Geophys. J. Int.,* **158**(3), 1009–1023.

Long, M.D., 2013. Constraints on subduction geodynamics from seismic anisotropy, *Rev. Geophys.,* **51**(1), 76–112.

Long, M.D. & Silver, P.G., 2008. The subduction zone flow field from seismic anisotropy: a global view, *Science,* **319**(5861), 315–318.

Long, M.D. & van der Hilst, R.D., 2006. Shear wave splitting from local events beneath the Ryukyu arc: trench-parallel anisotropy in the mantle wedge, *Phys. Earth planet. Inter.,* **155**(3), 300–312.

Lynner, C. & Long, M., 2014. Sub-slab anisotropy beneath the Sumatra and circum-Pacific subduction zones from source-side shear wave splitting observations, *Geochem. Geophys. Geosyst.,* **15**(6), 2262–2281.
Marson-Pidgeon, K. & Savage, M., 1997. Frequency-dependent anisotropy in Wellington, New Zealand, *Geophys. Res. Lett.,* **24**(24), 3297–3300.
Martin-Short, R., Allen, R.M. & Bastow, I.D., 2016. Subduction geometry beneath south central Alaska and its relationship to volcanism, *Geophys. Res. Lett.,* **43**(18), 9509–9517.
Martin-Short, R., Allen, R., Bastow, I.D., Porritt, R.W. & Miller, M.S., 2018. Seismic imaging of the Alaska subduction zone: implications for slab geometry and volcanism, *Geochem. Geophys. Geosyst.,* **19**(11), 4541–4560.
McPherson, A.M., Christensen, D.H., Abers, G.A. & Tape, C., 2020. Shear wave splitting and mantle flow beneath Alaska, *J. geophys. Res.,* **125**(4), doi:10.1029/2019JB018329.
Morley, A.M., Stuart, G.W., Kendall, J.-M. & Reyners, M., 2006. Mantle wedge anisotropy in the Hikurangi subduction zone, central North Island, New Zealand, *Geophys. Res. Lett.,* **33**(5), doi:10.1029/2005gl024569.
Müller, C., 2001. Upper mantle seismic anisotropy beneath Antarctica and the Scotia Sea region, *Geophys. J. Int.,* **147**(1), 105–122.
Nakajima, J. & Hasegawa, A., 2004. Shear-wave polarization anisotropy and subduction-induced flow in the mantle wedge of northeastern Japan, *Earth planet. Sci. Lett.,* **225**(3–4), 365–377.
Olive, J.-A., Pearce, F., Rondenay, S. & Behn, M.D., 2014. Pronounced zonation of seismic anisotropy in the Western Hellenic subduction zone and its geodynamic significance, *Earth planet. Sci. Lett.,* **391,** 100–109.
Piñero-Feliciangeli, L. & Kendall, J.-M., 2008. Sub-slab mantle flow parallel to the Caribbean plate boundaries: inferences from SKS splitting, *Tectonophysics,* **462**(1–4), 22–34.
Polet, J., Silver, P., Beck, S., Wallace, T., Zandt, G., Ruppert, S., Kind, R. & Rudloff, A., 2000. Shear wave anisotropy beneath the Andes from the BANJO, SEDA, and PISCO experiments, *J. geophys. Res.,* **105**(B3), 6287–6304.
Ratchkovski, N.A. & Hansen, R.A., 2002. New evidence for segmentation of the Alaska subduction zone, *Bull. seism. Soc. Am.,* **92**(5), 1754–1765.
Rossi, G., Abers, G., Rondenay, S. & Christensen, D., 2006. Unusual mantle Poisson's ratio, subduction, and crustal structure in central Alaska, *J. geophys. Res.,* **111**(B9), doi:10.1029/2005JB003956.
Saltzer, R.L., Gaherty, J.B. & Jordan, T.H., 2000. How are vertical shear wave splitting measurements affected by variations in the orientation of azimuthal anisotropy with depth?, *Geophys. J. Int.,* **141**(2), 374–390.
Sauber, J., Mcclusky, S. & King, R., 1998. Correction to 'Relation of ongoing deformation rates to the subduction zone process in southern Alaska', *Geophys. Res. Lett.,* **25**(2), 215–215.
Savage, M., 1999. Seismic anisotropy and mantle deformation: what have we learned from shear wave splitting?, *Rev. Geophys.,* **37**(1), 65–106.
Silver, P.G. & Chan, W.W., 1991. Shear wave splitting and subcontinental mantle deformation, *J. geophys. Res.,* **96**(B10), 16 429–16 454.
Smith, G.P., Wiens, D.A., Fischer, K.M., Dorman, L.M., Webb, S.C. & Hildebrand, J.A., 2001. A complex pattern of mantle flow in the Lau backarc, *Science,* **292**(5517), 713–716.
Song, T. & Kawakatsu, H., 2013. Subduction of oceanic asthenosphere: a critical appraisal in central Alaska, *Earth planet. Sci. Lett.,* **367,** 82–94.
Soto, G.L., Ni, J.F., Grand, S.P., Sandvol, E., Valenzuela, R.W., Speziale, M.G., González, J.M.G. & Reyes, T.D., 2009. Mantle flow in the Rivera–Cocos subduction zone, *Geophys. J. Int.,* **179**(2), 1004–1012.
Taira, A., 2001. Tectonic evolution of the Japanese island arc system, *Annu. Rev. Earth Planet. Sci.,* **29**(1), 109–134.
Teanby, N., Kendall, J.-M. & Van der Baan, M., 2004. Automation of shear-wave splitting measurements using cluster analysis, *Bull. seism. Soc. Am.,* **94**(2), 453–463.
Tian, Y. & Zhao, D., 2012. Seismic anisotropy and heterogeneity in the Alaska subduction zone, *Geophys. J. Int.,* **190**(1), 629–649.
Venereau, C.M.A., Martin-Short, R., Bastow, I.D., Allen, R.M. & Kounoudis, R., 2019. The role of variable slab dip in driving mantle flow at the eastern edge of the Alaskan subduction margin: insights from shear-wave splitting, *Geochem. Geophys. Geosyst.,* **20**(5), 2433–2448, doi:10.1029/2018GC008170.
Walpole, J., Wookey, J., Kendall, J.-M. & Masters, T.-G., 2017. Seismic anisotropy and mantle flow below subducting slabs, *Earth planet. Sci. Lett.,* **465,** 155–167.
Walsh, E., Arnold, R. & Savage, M., 2013. Silver and Chan revisited, *J. geophys. Res.,* **118**(10), 5500–5515.
Wirth, E. & Long, M., 2010. Frequency-dependent shear wave splitting beneath the Japan and Izu–Bonin subduction zones, *Phys. Earth planet. Inter.,* **181**(3–4), 141–154.
Yang, X., Fischer, K.M. & Abers, G.A., 1995. Seismic anisotropy beneath the Shumagin Islands segment of the Aleutian–Alaska subduction zone, *J. geophys. Res.,* **100**(B9), 18 165–18 177.
Zhang, S. & Karato, S., 1995. Lattice preferred orientation of olivine aggregates deformed in simple shear, *Nature,* **375**(6534), 774–777.

SUPPORTING INFORMATION

Supplementary data are available at *GJI* online.

Figure S1: High-quality splitting measurement example for station O19K. (a) Recorded seismograms filtered 0.1–1 Hz. (b) Two horizontal components rotated into radial and tangential directions—top two are originals and bottom two are corrected with splitting algorithm. In this example, the long axis of the anisotropy ellipse happens to align with the backazimuth. (c) Top: closer look at waveforms in the window; bottom: particle motion before and after correction (L–R). (d) Contour map with lines corresponding to one standard deviation. Thick line shows the 95 per cent confidence level for stability of a given measurement. (e and f) Variations in splitting measurements over different windows and during cluster analysis, respectively.
Figure S2: (a) Tectonic setting of south-central Alaska with major fault lines (Colpron *et al.* 2007), TA broad-band seismograph stations and earthquakes (circles) that produced high-quality splitting measurements. Solid arrows: absolute plate motion (APM) in the hot spot (HS) and no-net-rotation (NNR) reference frames (Gripp & Gordon 2002). Slab2.0 contours are after Hayes *et al.* (2018); major fault lines are after Colpron *et al.* (2007). (b) Local *S*-wave splitting measurements in south-central Alaska plotted at the station. (c) As per (b), but plotted at the ray-path midpoint. (d) Close-up of stations O19K and O20K plotted at the ray-path midpoint.
Figure S3: (a) Incidence angle (θ) for all splitting measurements. (b) Comparison of δt for $\theta < 20^\circ$ and $\theta \geq 20^\circ$.

Please note: Oxford University Press is not responsible for the content or functionality of any supporting materials supplied by the authors. Any queries (other than missing material) should be directed to the corresponding author for the paper.